Article

Highly Selective Colorimetric Sensor of Mercury(II) Ions by Andrographolide-Stabilized Silver Nanoparticles in Water and Antibacterial Evaluation

Chanon Talodthaisong, Pitiphoom Sangiamkittikul, Panupong Chongwichai, Apichart Saenchoopa, Saengrawee Thammawithan, Rina Patramanon, Suppanat Kosolwattana, and Sirinan Kulchat*

Read Online

ACCESS | Metrics & More | Article Recommendations | Supporting Information

ABSTRACT: Silver nanoparticles (AgNPs) are well known for their exceptional properties and versatility in various applications. This study used andrographolide as a biochemical stabilizer to synthesize AgNPs (andro-AgNPs). The andro-AgNPs were characterized by using UV−vis spectroscopy, revealing a surface plasmon resonance peak at 440 nm. Fourier transform infrared spectroscopy was also used to confirm the presence of AgNPs. Transmission electron microscopy was used to investigate the morphology of andro-AgNPs, which showed a spherical shape with an average diameter of 18.30 ± 5.57 nm ($n = 205$). Andro-AgNPs were utilized as a colorimetric sensor to detect mercury ions (Hg^{2+}) in water, and the optimized detection conditions were evaluated using UV−vis spectroscopy with a linear range of 15−

120 μM. The limit of detection and the limit of quantification for Hg^{2+} detection were found to be 11.15 and 37.15 μM, respectively. Furthermore, andro-AgNPs exhibited antibacterial properties against both Gram-positive (*Staphylococcus aureus*) and Gram-negative (*Escherichia coli*) bacteria. The results imply that andro-AgNPs hold promising potential for future biomedical applications.
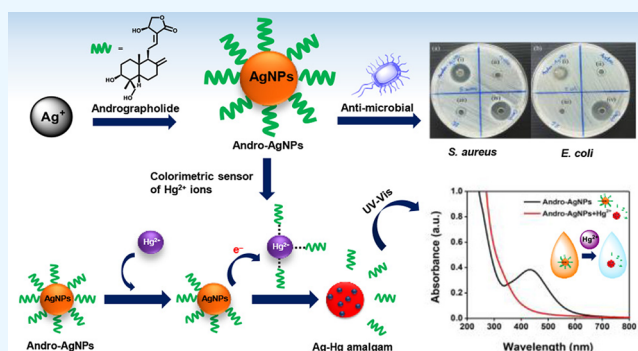
1. INTRODUCTION

In recent years, the detection of contamination by hazardous heavy metals in water and soil has become a significant and continuing challenge in environmental monitoring. While heavy-metal management is strictly regulated in many nations worldwide, the massively growing heavy-metal industry has made heavy-metal contamination a persistent issue.[1] Heavy metals like mercury (Hg), chromium (Cr), lead (Pb), arsenic (As), and cadmium (Cd) can damage and threaten natural ecosystems and human health.[2,3] Among these, mercury ions (Hg^{2+}) are one such potentially harmful pollutant that accumulates in marine organisms, water, and soil. The major source of Hg contamination is fuel burning electrical generation, but other sources, both natural and man-made, can also cause considerable contamination.[4] Even at very low dose levels, Hg exposure can cause serious health problems in humans and animals that consume contaminated foods. It can cause disorders, such as autism hypoesthesia, ataxia, rheumatoid arthritis, Parkinson's disease, Alzheimer's disease, dysarthria, and hearing impairment, by affecting the neurological, renal, cardiovascular, immunological, and reproductive systems.[5] Therefore, the assessment of Hg^{2+} in the environment, especially in drinking water at concentrations relevant to human health, remains a critical concern.

A variety of analytical methods have been developed to detect and monitor the contaminating level of Hg(II) ions in the environment, such as atomic fluorescence spectroscopy,[6] flame atomic absorption spectroscopy,[7] graphite furnace atomic absorption spectroscopy,[8] high-performance liquid chromatography,[9] and fluorescence,[10,11] electrochemical,[12,13] and colorimetric methods.[14,15] However, it is highly desirable to monitor the presence of Hg^{2+} in the environment and drinking water samples in a timely, sensitive, selective, and accurate manner. Among the previously described methods, colorimetric approaches have been recognized as methods that are appealing having a rapid response, with high sensitivity, being inexpensive, and are accessible sensors that can be used in field work.[16]

Various colorimetric probes based on nanoparticles for the detection of Hg^{2+} have been developed, for example, using gold (Au) nanoparticles,[17] silver nanoparticles (AgNPs),[18]
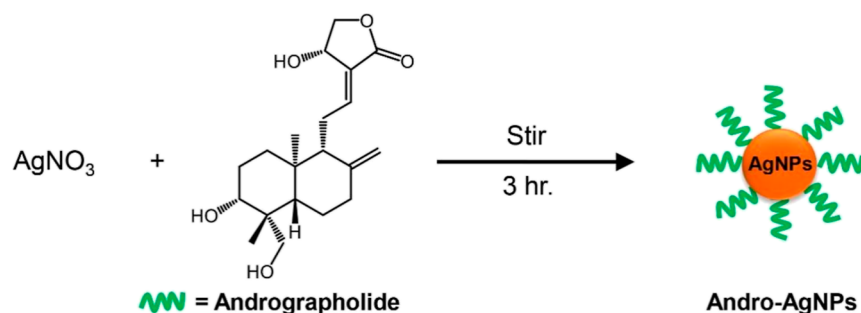
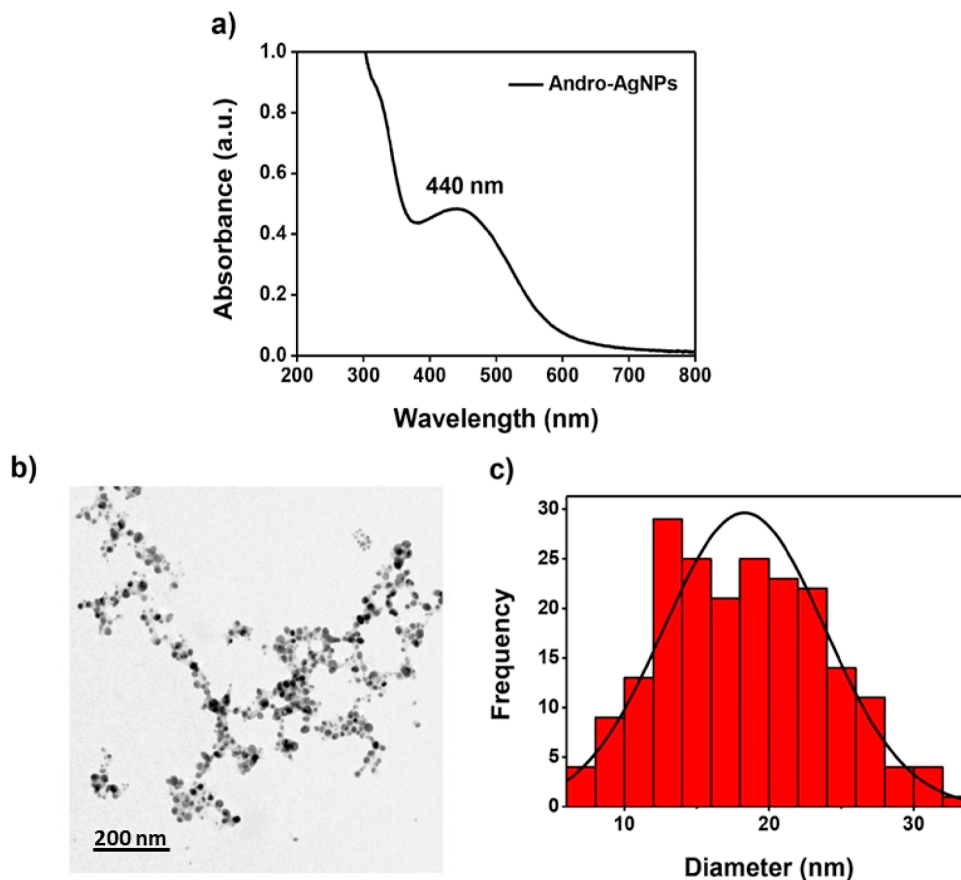**Figure 1.** Synthesis of AgNPs using andrographolide as a reducer and a stabilizer.

Figure 2. (a) UV−vis absorption spectra, (b) TEM image, and (c) size distribution plot of andro-AgNPs from TEM ($n = 205$).

copper nanoparticles,[19] and nanoclusters.[20] Over recent decades, the use of AgNPs has risen in a wide range of fields, such as biotechnologies,[21,22] nanodevices,[23] energy storage,[24,25] catalysis,[26] biomedical applications,[27] and sensors.[28−30] Furthermore, AgNPs are less harmful to mammalian cells than other metal nanoparticles,[31] and due to their tiny size, they can easily infiltrate the cell membrane and function as a potential antimicrobial agent.[32] Synthesis of AgNPs can be performed by various approaches, such as photochemical,[33] biological,[34] physical,[35] and chemical methods.[36] AgNPs are being functionalized based on their application in sensor technology for the detection of Hg,[37−39] with an emphasis on eco-safety considerations.[40,41]

In this work, AgNPs were synthesized using andrographolide as a stabilizer.[42] The synthesis and utilization of andrographolide-stabilized AgNPs (andro-AgNPs) have been previously investigated with respect to their antimicrobial activity and mode of action, as reported in a published research study.[42] In the previous work, the antimicrobial potential of andro-AgNPs was explored, highlighting their efficacy against bacterial infections of *Burkholderia pseudomallei*. Motivated by the promising results from the aforementioned study, we sought to further investigate the subsequent applications of andro-AgNPs. In our current research, we focus on utilizing the same antimicrobial andro-AgNPs as colorimetric sensors for the detection of Hg. As a novelty, in our work, we emphasize additional eco-safety considerations in functionalizing AgNPs using andrographolide for sensor technology. This emphasis on safety and environmental impact is a valuable aspect of this research. Our study addresses the issue of heavy-metal pollution in water and soil. However, there have been other recent studies and developments in this area that we consider to have research gaps. Additionally, while we believe that our study covers analytical methods for detecting Hg^{2+}, there are

some restrictions, including those related to sensitivity, specificity, and long-term stability. By repurposing the andro-AgNPs, we aim to demonstrate their versatility and expand their scope of applications.

Andrographolide is a labdane diterpenoid produced by the plant *Andrographis paniculata* that possesses a variety of medicinal applications, such as anti-inflammatory and anti-platelet aggregation activity as well as potential antineoplastic effects.[43] The colorimetric sensor along with andro-AgNPs was created to detect Hg^{2+} based on the interactions of Hg^{2+} with the hydroxyl ligands of andrographolide bound to AgNPs. Then, the oxidized andrographolide was released from the Ag surface, and the original yellowish-orange solution turned colorless due to a possible redox interaction between Hg and Ag atoms. The intensity of color changes can be observed based on the concentrations of Hg^{2+} added to the solutions. Not only can our suggested andro-AgNPs be used to detect Hg^{2+} but they have also been proven to possess antibacterial activity against both Gram-positive (*Staphylococcus aureus*) and Gram-negative (*E. coli*) bacteria. As a result, andro-AgNPs may be an appropriate component of selective and rapid visual Hg^{2+} sensors with potential biomedical applications.

2. RESULTS AND DISCUSSION

2.1. Synthesis of Andro-AgNPs.[42]
Andro-AgNPs were synthesized by using a chemical reduction method with andrographolide, an organic compound that can reduce and stabilize AgNPs. The synthesis involved only a few chemicals and was conducted by stirring the mixture of andrographolide and $AgNO_3$ at room temperature for 3 h (Figure 1). The optimal condition for synthesizing andro-AgNPs was to use 3 mL of an andrographolide solution with 3 mL of 20 mM $AgNO_3$. This condition produced the highest light absorbance and the lowest wavelength of the absorbed light, resulting in a narrower size distribution of andro-AgNPs. The absorbance calculation showed that the molar concentration of the AgNPs was 7.809 nM, as discussed in Section 4.2.

2.2. Characterization of Andro-AgNPs.
The andro-AgNPs underwent characterization through UV–vis spectroscopy, which revealed a strong surface plasmon resonance (SPR) band as a broad characteristic absorption peak at 440 nm (Figure 2a), indicating varying sizes of AgNPs. The morphology and size of the andro-AgNPs were determined through transmission electron microscopy (TEM), which showed a uniform dispersion of homogeneous, spherical-shaped AgNPs (Figure 2b). The size distribution of the AgNPs was determined by counting the AgNPs visible in the TEM image, as shown in Figure 2c, using ImageJ software. The average diameter of andro-AgNPs was found to be 18.30 ± 5.57 nm ($n = 205$).

The functional groups of andrographolide's capsule, synthesized andrographolide, and andro-AgNPs were analyzed using Fourier transform infrared (FT-IR) spectroscopy.[42] The FT-IR spectrum of andrographolide's capsule exhibited characteristic peaks at 1050 and 1060 cm^{-1}, indicating the C–O stretching of andrographolide.[44] Peaks at 1350 and 1450 cm^{-1} indicated the C=O stretching of the ester function/carboxyl group and the C–H bending of the andrographolide molecules, respectively. The peak at 2900 cm^{-1} indicated the C–H stretching and the peak at 3300 and 3400 cm^{-1} corresponded to the O–H stretching of all hydroxyl groups in the andrographolide molecules. The FT-IR spectrum of the synthesized andrographolide revealed additional peaks at 1400

and 1600 cm^{-1}, corresponding to the bending of the C–H alkane group and the stretching of the C=C alkene group, respectively. The FT-IR spectrum of andro-AgNPs was similar to that of andrographolide, with reduced peak intensities at 1350 cm^{-1} (O–H bending) and 1050 cm^{-1} (C–O stretching) due to the bonding and stabilization of the Ag^0 nanoparticles in the solution. The zeta potential of andro-AgNPs was -21.20 ± 0.56 mV, indicating uniform dispersion and stable colloidal AgNPs. Dynamic light scattering (DLS) showed an average hydrodynamic diameter of 63.27 ± 0.82 nm, which may suggest the aggregation of andro-AgNPs in the solution due to the functional groups of the andrographolide stabilizers.

2.3. Proposed Andro-AgNPs Mechanism for Hg^{2+} Detection via UV–Vis Spectroscopy.
UV–vis spectroscopy was used to observe the interaction between andro-AgNPs and Hg^{2+}. As depicted in Figure 3, the presence of Hg^{2+} in the
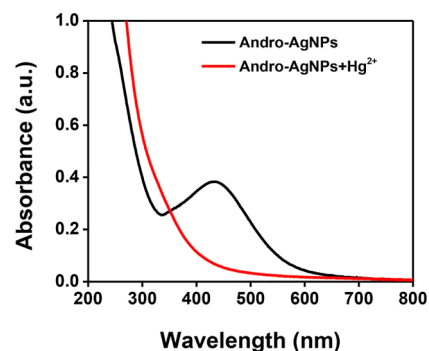

Figure 3. UV–vis absorption spectra of andro-AgNPs and andro-AgNPs + Hg^{2+}.

andro-AgNPs solution resulted in a reduction of the absorption peak at 430 nm, leading to its disappearance and a color change from yellowish orange to colorless. Similar results have been reported in many other studies[45,46] involving the interaction of AgNPs and Hg^{2+} due to the oxidation of the nanoparticles.

Some literature has reported that Hg^{2+} can interact with the functional groups (e.g., carboxyl, hydroxyl, and thiol groups) of the stabilizers on the surface of Ag or Au NPs.[47,48] Therefore, the color change from orange to colorless of andro-AgNPs–Hg^{2+} can be explained by the proposed mechanism, as shown in Figure 4. First, the Hg^{2+} interact with the hydroxyl group of andrographolide bound to AgNPs. Then, Hg^{2+} react with Ag atoms and a redox reaction occurs due to the standard potential of Ag being lower than that of Hg (E^0 of $Ag^+/Ag = 0.80$ V and E^0 of $Hg^{2+}/Hg = 0.85$ V). Therefore, an Ag/Hg amalgam alloy is formed in the solution that can no longer absorb light, so the AgNPs and the solution become colorless. The formation of amalgam alloy is presented as shown in eq 1. This proposed mechanism enables the detection of Hg^{2+} after optimizing different conditions, such as reaction time, andro-AgNPs concentrations, and selective detection with various metal ions. Also, the amalgam alloy was confirmed by the DLS technique. The hydrodiameter size of andro-AgNPs increased from 63.27 ± 0.82 nm to 109.80 ± 1.47 nm in the presence of Hg^{2+}, suggesting that an Ag–Hg amalgam had occurred as depicted in Figure 4. In fact, it has been documented in the literature[49,50] that the stable surface coating on AgNPs acts as a protection against Ag passivation and oxidation and, consequently, for AgNPs exposed to Hg^{2+} and the Ag–Hg
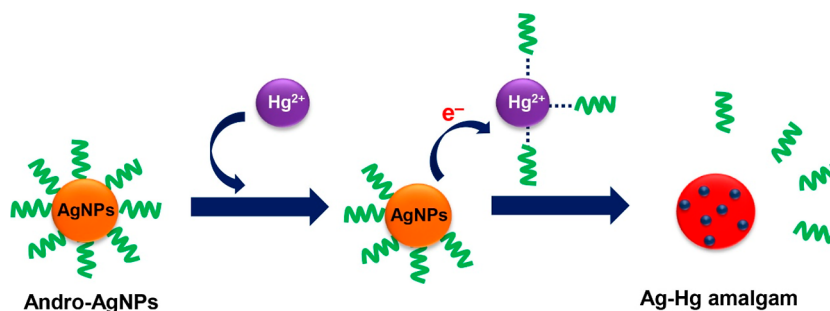
Figure 4. Schematic representation of the sensing mechanism of Hg^{2+} and andro-AgNPs.
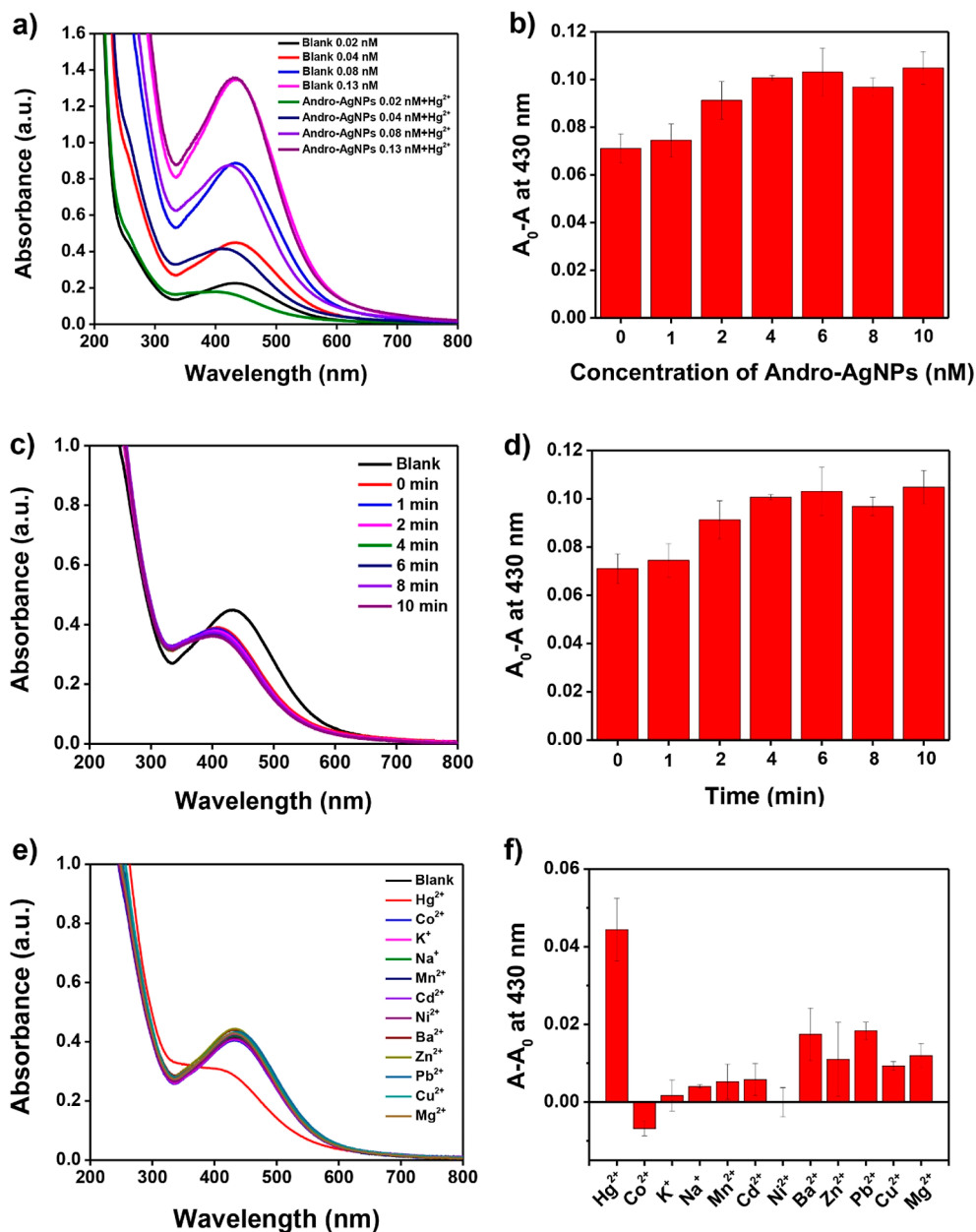

Figure 5. (a) UV–vis absorption spectra for various andro-AgNPs concentrations interacting with Hg^{2+} and (b) the corresponding relative change of the absorbance of andro-AgNPs at 430 nm with respect to the andro-AgNPs concentration in the presence of 20 μM Hg^{2+}, (c) the corresponding UV–vis absorption spectra of andro-AgNPs at 430 nm with respect to time in the presence of 0.08 nM Hg^{2+}, (d) relative change in the absorbance of andro-AgNPs for the data in (c),(e) UV–vis absorption spectra of andro-AgNPs at 430 nm in the presence of 20 μM Hg^{2+} and various metal ions, and (f) relative change of the absorbance of andro-AgNPs for the data in (e).

Figure 6. (a) Comparison of colorimetric responses for 0.08 nM andro-AgNPs in the presence of 20 μM of various metal ions. (b) Colorimetric response to different concentrations of Hg^{2+} (from left to right: 0, 0.1 0.15, 0.20, 0.25, 0.30, and 0.50 mM).
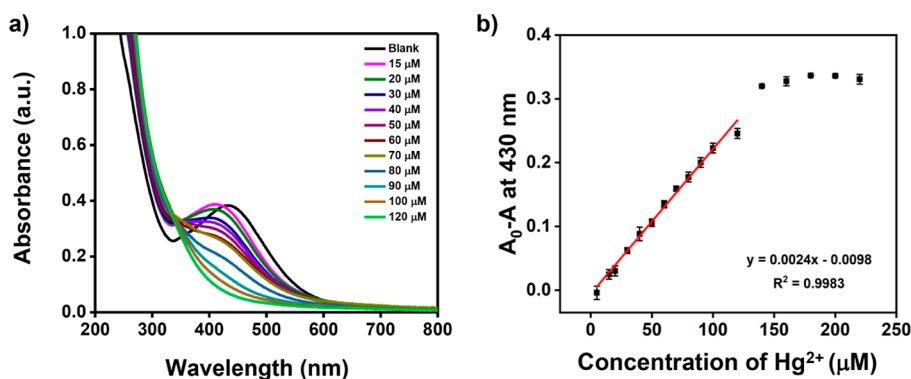

Figure 7. (a) UV−vis absorption spectra of 0.08 nM andro-AgNPs treated with various concentrations of Hg^{2+} ranging from 15 to 120 μM, (b) absorbance ratio ($A_0 - A$) at 430 nm plotted against Hg^{2+} concentrations, where "A_0" represents the absorbance of andro-AgNPs (blank) and "A" represents the absorbance of andro-AgNPs in the presence of Hg^{2+} concentrations ranging from 15 to 120 μM.

interaction, results in an Ag/Hg amalgam. Moreover, the zeta potentials of the andro-AgNPs solution increased from −21.20 ± 0.56 to −18.60 ± 1.74 mV in the presence of Hg^{2+} due to the formation of the complexation between Hg^{2+} and andrographolide. Following the addition of Hg^{2+}, as shown in Figure S1a,b, the formation of the andro-AgNPs−Hg^{2+} complex became larger, and particle agglomeration could be seen with an average diameter of 44.94 ± 7.73 nm (n = 45), in accordance with the zeta potential data. Additionally, the elemental compositions of andro-AgNPs−Hg^{2+} were examined by energy-dispersive X-ray analysis (EDX). The results depicted in Figure S1c revealed the peaks arising from Ag and Hg at approximately 3 keV,[51] confirming the presence of Ag and Hg in andro-AgNPs−Hg^{2+}. A peak for elemental copper (Cu) was visible and was attributed to the carbon-supported copper grid employed to prepare the sample.

$$\text{Andro} - \text{AgNPs} + Hg^{2+}$$
$$\rightarrow \text{Ag} - \text{Hg(amalgam)} + \text{Andro} - Hg^{2+} \qquad (1)$$
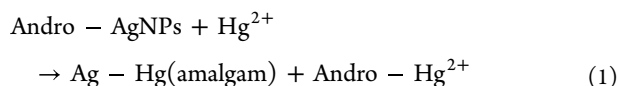
2.4. Optimizing the Andro-AgNPs Concentration, Reaction Time, and Selectivity for Hg^{2+} Detection. Optical sensing studies were conducted to determine the optimal concentration of andro-AgNPs for detecting Hg^{2+}. Several concentrations of andro-AgNPs (0.02, 0.04, 0.08, and 0.13 nM) were added to 20 μM Hg^{2+} solutions. The absorption spectra results, shown in Figure 5a,b, indicate that higher andro-AgNPs concentrations lead to greater interaction with Hg^{2+} and the absence of the spectra. The maximum

absorbance change ratio at 430 nm ($A_0 - A$) was observed at a 0.08 nM concentration, which was selected for further studies. The optimal reaction time for andro-AgNPs and Hg^{2+} was investigated by using an andro-AgNPs concentration of 0.08 nM in 20 μM Hg^{2+} solutions. The color of the mixing solution of andro-AgNPs and Hg^{2+} changed from yellowish orange to colorless instantly (Figure 6a), as observed at different incubation times ranging from 1 to 10 min, as shown in Figure 5c,d. The absorbance change ratio at 430 nm stabilized after 6 min of reaction time, indicating a suitable condition for further studies.

The selectivity of andro-AgNPs to interact with Hg^{2+} was evaluated by comparing the reactions of andro-AgNPs with other transition metals, alkalis, and alkaline earth metal ions (Na^+, K^+, Ca^{2+}, Mg^{2+}, Ba^{2+}, Pb^{2+}, Mn^{2+}, Ni^{2+}, Cu^{2+}, Zn^{2+}, Cd^{2+}, and Co^{2+}) using UV−vis spectroscopy, as shown in Figure 5e,f. The absorbance change ratio ($A - A_0$ at 430 nm) of the andro-AgNPs and Hg^{2+} reaction presents the most significant interaction, while there were no notable outcomes from the interactions of andro-AgNPs with other cations.

2.5. Colorimetric Sensing of Andro-AgNPs with Various Metal Ions and Hg^{2+} Based on Naked-Eye Detection. The colorimetric responses of andro-AgNPs with different cations were evaluated using naked-eye observation (Figure 6a). The results show that only the solution of andro-AgNPs and Hg^{2+} changed from yellowish orange to colorless, while the other solutions remained unchanged. The minimum concentration of metal ions at which the color change could be observed with the naked eye after adding andro-AgNPs was

0.08 nM. Thus, it can be concluded that andro-AgNPs are more specifically sensitive and selective to reacting with Hg^{2+} than other metal ions. The presence of Hg^{2+} in the solution can be observed simply by the colorimetric response of andro-AgNPs with the naked eye. The yellowish-orange color of the andro-AgNP solution disappeared gradually with an increasing Hg^{2+} concentration, as shown in Figure 6b. Therefore, the amount of Hg^{2+} can be estimated by observing the different colors of the solution. The maximum concentration of Hg^{2+} at which the solution became completely colorless was around 0.50 mM. This colorimetric phenomenon could be useful for quickly sensing Hg^{2+} in general water samples.

2.6. Assessing the Optical Sensor's Analytical Capability in Detecting Hg^{2+}. In this section, various concentrations of Hg^{2+} were quantitatively investigated using andro-AgNPs (as shown in Figure 7a,b). The absorption peak of the andro-AgNP solution at 430 nm was selected as the detection wavelength to estimate the degree of conversion from AgNPs to Ag ions. First, a standardized curve between the change in absorbance ratio and Hg^{2+} concentration was constructed (as shown in Figure 7b). The optimal conditions from the previous experimental sections, including the concentration of andro-AgNPs (0.08 nM), the range of Hg^{2+} concentrations (15−120 μM), and the reaction time (6 min), were applied. The standardized curve showed that the absorbance change ratio was linearly proportional to the amount of Hg^{2+}. The relationship between them was depicted as a linear regression equation, $(A_0 - A)/A_0 = 0.0024x - 0.0098$, with a correlation coefficient squared (R^2) of 0.9983, where "A_0" represents the absorbance of andro-AgNPs (blank) and "A" represents the absorbance of andro-AgNPs in the presence of different concentrations of Hg^{2+}. Finally, the limit of detection (LOD) and the limit of quantitation (LOQ) were estimated to be 11.15 and 37.15 μM, respectively. The absorbance change ratio $(A_0 - A/A_0)$ at 430 nm was equal to 3 standard deviations [3 r; 10 replicate measurements of the blank sample (A_0)] and 10 standard deviations [(10 r) of A_0 for LOQ].

2.7. Application of Andro-AgNPs for the Determination of Hg^{2+} Ions in Real-Water Samples. The efficiency of the colorimetric sensor for detecting Hg^{2+} in commercial drinking water was evaluated. To calculate the concentration of Hg^{2+} and the recovery percentages, the standard addition method was used with known spiked samples of 40 and 60 μM of Hg^{2+}. The results show that the sensor had acceptable detection values, with a recovery rate of 93.12 ± 2.31 to 95.61 ± 1.07% and a relative standard deviation (RSD) of 1.12−2.48%, as summarized in Table 1.

2.8. Comparison with Other Methods for Hg^{2+} Determination. Hg contamination is a significant concern for human health and the environment, and its presence in drinking water has been a worldwide issue. WHO has

recommended that Hg in drinking water should not contribute more than 0.4 mg to the total daily intake, and the maximum allowable limit level of Hg^{2+} in drinking water is defined as 1 μg/L (approximately 0.005 μM).[52] Therefore, it is essential to detect the presence of Hg^{2+} in aqueous solutions, particularly in drinking water, at relatively low concentrations. Several methods for detecting Hg^{2+} at low concentrations have been developed, and some of them are listed in Table 2. Among these methods, the colorimetric method has gained the most interest due to its simplicity of use, low cost, few requirements for the preparation process, and low reaction time for measurements. Additionally, colorimetric techniques produce significant color changes that are visible to the unaided eye.

2.9. Comprehensive Assessment of Antibacterial Activities. To evaluate the antimicrobial activity of andro-AgNPs, both diffusion tests and broth microdilution methods were employed, as described in Section 4.7. The preliminary screening via the diffusion test showed that andro-AgNPs exhibited antimicrobial activity against all test bacteria, whereas andrographolide did not inhibit any of them. After the screening, the antimicrobial susceptibility of andro-AgNPs was determined using a microdilution method, as illustrated in Figure 8. The minimum inhibitory concentration (MIC) and minimum bactericidal concentration (MBC) were determined to identify the lowest concentration of andro-AgNPs required to inhibit or kill bacteria. The MIC and MBC values of andro-AgNPs against *Escherichia coli* O157:H7 and *S. aureus* ATCC 25923 were found to be 0.028 nM, as shown in Table 3. The results indicate that andro-AgNPs exhibit excellent antibacterial activity, as demonstrated by their low MIC and MBC values in the nM range. This is consistent with previous studies that evaluated the antimicrobial activity of AgNPs synthesized using *Andrographis paniculata* extract.[42,65] Those studies showed that the AgNPs were effective against a variety of bacteria, including *S. aureus*, *E. coli*, *B. pseudomallei*, Lactobacillus, Enterococcus, *Staphylococcus typhi*, *Staphylococcus pyogenes*, *V. cholera*, and *Klebsiella pneumonia*. This suggests that the AgNPs synthesized using andrographolide as a stabilizer could serve as an effective antimicrobial agent against both Gram-negative and Gram-positive bacteria and may prove useful in combating human pathogens.

3. CONCLUSIONS

In this study, simple and effective andro-AgNPs were successfully synthesized and used to detect Hg^{2+} by exploiting their interaction with AgNPs. We optimized the detection of Hg^{2+} by assessing the concentration of andro-AgNPs and the reaction time. Our colorimetric sensing system was selectively able to detect Hg^{2+} compared to other metal ions in a relatively very short time of only 6 min. The color changes from yellowish orange to colorless were easily observed with the naked eye, and the intensity of the color change was based on the concentration of Hg^{2+} added. UV−vis spectrometry was also used to quantify Hg^{2+} concentrations over a linear range of 15−120 μM, with a LOD and limit of quantitation (LOQ) of 11.15 and 37.15 μM, respectively. Our proposed rapid and simple colorimetric sensor was able to detect Hg^{2+} in real water samples using a standard addition method with satisfactory results. Furthermore, the andro-AgNPs possessed antimicrobial activity against both Gram-positive and Gram-negative bacteria. This andro-AgNP sensor could potentially be used in the environmental sensing and biomedical fields in the future.

Table 1. Determination of Hg^{2+} Concentrations in Real-Water Samples

water sample	Hg^{2+} added (μM)	proposed method ($n = 3$)		RSD (%)
		Hg^{2+} found (μM)	% recovery ± SD	
commercial drinking water	40	38.25 ± 0.43	95.61 ± 1.07	1.12
	60	55.87 ± 1.38	93.12 ± 2.31	2.48

Table 2. Comparison of Different Hg^{2+} Sensing Methods

| methods	materials	linear range (μM)	detection limit (μM)	ref
electrochemistry	AgNWs/HPMC/chitosan/urease/SPCE	5–25	3.94	[53]
	Au-modified screen-printed carbon electrode (Au-SPCE)	0.004–0.368	0.0029	[54]
	calixarene bulk-modified screen-printed electrodes (SPCEs)	0.368–8.840	0.177	[55]
	thiol-functionalized oligonucleotide immobilized on a screen-printed Au electrode (SPGE)	0.001–10	0.0006	[56]
Fluorescence	graphene quantum dots	10–100	0.0900	[57]
	Ce ions doped on ZnS quantum dots (ZnS/Ce QDs)	10–100	0.8200	[58]
	lysosome-targetable fluorescence sensor (Lyso-HGP)	0.005–5	0.0068	[59]
	embonic acid-functionalized AgNPs	0.001–0.01	0.005	[60]
Colorimetric	cysteine-modified Au–Ag core–shell nanorods	1–60	0.273	[61]
	carrageenan-stabilized AgNP gel probe kit	500–2500	292	[62]
	peptide-conjugated AgNPs	1–100	4.125	[63]
	GABA-Cit AgNPs	5–35	2.37	[64]
	andro-AgNPs	15–120	11.15	this work
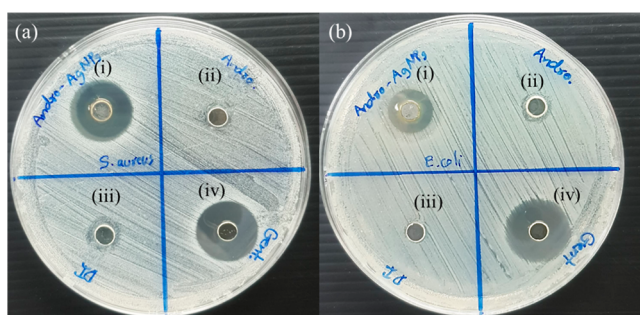
Figure 8. Andro-AgNPs and their antimicrobial activity. Antimicrobial activity of position (i) andro-AgNPs, position (ii) andrographolide, position (iii) DI water, and position (iv) gentamicin 33.5 μM against (a) *S. aureus* and (b) *E. coli*.

Table 3. Inhibition Zone, MIC, and MBC of Andro-AgNPs against Gram-Positive and Gram-Negative Bacteria

bacteria	inhibition zone (mm)	MIC (nM)	MBC (nM)
E. coli O157/H7	12.67 ± 0.29	0.028	0.028
S. aureus ATCC 25923	17.33 ± 0.29	0.028	0.028

4. EXPERIMENTAL SECTION

4.1. Materials. Andrographolide (9 mg/capsule) was purchased from Khaolaor, Ltd., Samut Prakan, Thailand. Silver nitrate (99.9%) was purchased from POCH, Poland. Copper-(II) nitrate trihydrate [Cu (NO$_3$)$_2$·3H$_2$O, $\geq$ 99%] and zinc nitrate hexahydrate [Zn(NO$_3$)$_2$·6H$_2$O, $\geq$ 99%] were purchased from Fluka, Switzerland. Magnesium nitrate [Mg-(NO$_3$)$_2$, 99.4%], sodium nitrate (NaNO$_3$, $\geq$ 99%), barium nitrate (Ba(NO$_3$)$_2$, $\geq$ 99%), and cobalt(II) nitrate hexahydrate [Co(NO$_3$)$_2$·6H$_2$O, $\geq$ 98%] were purchased from Univar, Australia. Sodium hydroxide anhydrous (NaOH, 99%), lead(II) nitrate [Pb(NO$_3$)$_2$, 99%], nickel(II) nitrate hexahydrate [Ni(NO$_3$)$_2$·6H$_2$O, 99%], and cadmium nitrate tetrahydrate [Cd(NO$_3$)$_2$·4H$_2$O, 99%] were purchased from Carlo Erba, Italy. Manganese(II) nitrate tetrahydrate [Mn(NO$_3$)$_2$·4H$_2$O, $\geq$ 97%] was purchased from Sigma-Aldrich, China. Hg(II) chloride (HgCl$_2$, $\geq$ 99.5%) was purchased from QRec, New Zealand. Deionized water (DI) with a specific resistivity of 18.2 MΩ. cm was obtained from a RiOs Type I Simplicity 185 (Millipore) water purification system. Dimethyl sulfoxide was purchased from Riedel-deHaën, Germany. Antimicrobial activity assays used *E. coli* (*E. coli*, O157H7) and *S. aureus* (*S.*

aureus ATCC25923), which were obtained from the Biochemistry Laboratory, Biochemistry Department, Faculty of Science, Khon Kaen University, Thailand.

4.2. Synthesis of Andro-AgNPs. The andro-AgNPs were prepared via modifying a previously reported method.[42] We started with the preparation of an andrographolide broth. Briefly, 180 mg of andrographolide (20 capsules) was dissolved in 60 mL of DI water and stirred at room temperature for 1 h. After that, the andrographolide solution was filtered with Whatman paper number 1. The filtrate was collected and filtered again by a microfilter to obtain andrographolide broth. To prepare andro-AgNPs, 3 mL of andrographolide broth was mixed with 24 mL of DI water in a 100 mL Erlenmeyer flask. Then, 3 mL of 20 mM silver nitrate (AgNO$_3$) was added, and the solution was stirred vigorously for 3 h at room temperature. The solution changed from yellow to reddish brown, indicating the formation of andro-AgNPs. The molar concentration (c) of andro-AgNPs was estimated to be 7.809 nM, using an extinction coefficient (ε) of 31.3 × 10^8 M^{-1} cm^{-1} at 440 nm (the absorption "A" at the particles measured λ_{max}) for 18 nm diameter (d) citrate-AgNPs[66] according to the Beer–Lambert law ($c = A/\varepsilon d$).

4.3. Characterization of Andro-AgNPs and Sensing Investigations. UV–vis spectra were recorded using an Agilent Technologies Cary 60 UV–vis spectrophotometer with 1.0 cm path length quartz cells, covering a range of 200–800 nm. For the measurement, 300 μL of andro-AgNPs with a concentration of 0.026 nM was diluted with DI water to 5 mL. The morphology and elemental composition of the AgNPs were determined by using a Tecnai G2 20 S-TWIN transmission electron microscope, at an acceleration voltage of 200 kV, and EDX analysis, respectively. The surface functional groups on the nanoparticles were determined by attenuated total reflection (ATR)–FTIR scanning from 4000 to 600 cm^{-1} using a Bruker TENSOR 27 system. The hydrodynamic size of the nanoparticles of AgNPs was determined using DLS, and the particle charge potential was evaluated by electrophoretic light scattering, using a Malvern Zetasizer Nano series (Nano ZS, Worcestershire, UK).

4.4. Visual Colorimetric Sensing of Hg^{2+} Using Andro-AgNPs. Andro-AgNPs were utilized as nanosensor probes for the colorimetric sensing of Hg^{2+} at room temperature, which is the most stable inorganic form of Hg found in aquatic environments.[67] First, 300 μL of andro-AgNPs was added to a vial, followed by the addition of a stock solution of Hg^{2+} in

water. The concentration of Hg^{2+} was adjusted using DI water to achieve different final concentrations of 0, 0.1, 0.15, 0.20, 0.25, 0.3, and 0.5 mM. The color changes of the solutions were then observed with the naked eye.

4.5. Preparation of Selectivity Studies and Naked-Eye Detection of Hg^{2+}. To prepare each vial sample, 1000 μL of andro-AgNP solution (0.08 nM) and 2 mL of DI water were added. Then, 250 μL of a stock solution of each ion (Hg^{2+}, Na^+, K^+, Ca^{2+}, Mg^{2+}, Ba^{2+}, Pb^{2+}, Mn^{2+}, Ni^{2+}, Cu^{2+}, Zn^{2+}, Cd^{2+}, and Co^{2+}) was mixed into the vial, resulting in a final concentration of 20 μM. The mixed solution volume in each vial was adjusted to 5 mL before the absorbance was determined using UV−vis spectroscopy. Additionally, the color change of each solution was observed with the naked eye.

4.6. Determination of Hg^{2+} Ions in Real-Water Samples. To prepare the real water samples, commercial drinking water was spiked with 40 and 60 μM Hg^{2+} solution. The sensing experiments, similar to those described in Sections 2.4 and 2.5, were then conducted to develop a standard curve for estimating Hg^{2+} in the unknown samples.

4.7. Antimicrobial Activity. *4.7.1. Antibacterial Screening by Well Diffusion.* The antimicrobial screening tests were conducted using the diffusion method. A single colony was grown in Mueller Hinton Broth (MHB) at 37 °C for 24 h. The bacteria were then diluted in the same media to an inoculum of 1×10^6 CFU/mL. Andro-AgNPs were added to 6 mm diameter wells on a three-dimensional MH agar plate at 30 μL and then incubated at 37 °C for 24 h. The positive control was gentamicin, while DI water was the negative control. The inhibition zones were observed after 24 h of incubation.

4.7.2. MICs and MBCs by the Broth Microdilution Method. The broth microdilution method was used to determine the MICs and MBCs of andro-AgNPs. A range of concentrations of andro-AgNPs were prepared by 2-fold serial dilution. Next, the solutions were added to an equal volume of bacterial suspension (50 μL) in each well of a 96-well plate, with the final cell concentration ranging from 1×10^6 to 1×10^7 CFU/mL. The plates were incubated at 37 °C for 24 h. The MIC was determined as the lowest concentration of andro-AgNPs that inhibited the growth of bacteria (preventing the appearance of turbidity). The MBC was defined as the lowest concentration of andro-AgNPs that completely killed the bacteria. To perform the MBC test, the suspension from the MICs was plated onto solid media and incubated at 37 °C for 24 h. The MBC value was taken as the lowest concentration that produced no colonies on the agar plates.

■ ASSOCIATED CONTENT

Data Availability Statement

The authors confirm that the data supporting the findings of this study are available within the article. Upon reasonable request, raw data that support the findings of the study are available from the corresponding author.

ⓘ Supporting Information

The Supporting Information is available free of charge at https://pubs.acs.org/doi/10.1021/acsomega.3c03789.

TEM image, size distribution plot, and EDX spectrum of andro-AgNPs−Hg^{2+} (PDF)

■ AUTHOR INFORMATION

Corresponding Author

Sirinan Kulchat − *Department of Chemistry, Faculty of Science, Khon Kaen University, Khon Kaen 40002, Thailand; Materials Chemistry Research Center, Department of Chemistry and Center of Excellence for Innovation in Chemistry, Faculty of Science, Khon Kaen University, Khon Kaen 40002, Thailand;* ⓞ orcid.org/0000-0002-2411-7495; Email: sirikul@kku.ac.th

Authors

Chanon Talodthaisong − *Department of Chemistry, Faculty of Science, Khon Kaen University, Khon Kaen 40002, Thailand; Materials Chemistry Research Center, Department of Chemistry and Center of Excellence for Innovation in Chemistry, Faculty of Science, Khon Kaen University, Khon Kaen 40002, Thailand*

Pitiphoom Sangiamkittikul − *Department of Chemistry, Faculty of Science, Khon Kaen University, Khon Kaen 40002, Thailand*

Panupong Chongwichai − *Department of Chemistry, Faculty of Science, Khon Kaen University, Khon Kaen 40002, Thailand*

Apichart Saenchoopa − *Department of Chemistry, Faculty of Science, Khon Kaen University, Khon Kaen 40002, Thailand; Materials Chemistry Research Center, Department of Chemistry and Center of Excellence for Innovation in Chemistry, Faculty of Science, Khon Kaen University, Khon Kaen 40002, Thailand*

Saengrawee Thammawithan − *Department of Biochemistry, Faculty of Science, Khon Kaen University, Khon Kaen 40002, Thailand*

Rina Patramanon − *Department of Biochemistry, Faculty of Science, Khon Kaen University, Khon Kaen 40002, Thailand*

Suppanat Kosolwattana − *Department of Chemistry, Faculty of Science, Khon Kaen University, Khon Kaen 40002, Thailand; Materials Chemistry Research Center, Department of Chemistry and Center of Excellence for Innovation in Chemistry, Faculty of Science, Khon Kaen University, Khon Kaen 40002, Thailand*

Complete contact information is available at:
https://pubs.acs.org/10.1021/acsomega.3c03789

Author Contributions

Conceptualization: S.K*., C.T., P.S., and P.C.; methodology: C.T., P.S., P.C., A.S., and S.T.; validation: S.K*., S.K., and R.P.; formal analysis: S.K*., C.T., P.S., P.C., A.S., and S.T.; investigation: S.K*., C.T., P.S., P.C., A.S., S.T., P.P., and S.K.; photorecording: S.K., C.T., P.S., and P.C.; writing−original draft preparation: S.K., C.T., P.S., and P.C.; and writing−review and editing, visualization, supervision, and project administration: S.K*. All authors have read and agreed to the published version of the manuscript.

Notes

The authors declare no competing financial interest.

Science, Khon Kaen University, and the Center of Excellence for Innovation in Chemistry (PERCH–CIC), Ministry of Higher Education, Science, Research and Innovation.

■ REFERENCES

(1) Qing, X.; Yutong, Z.; Shenggao, L. Assessment of Heavy Metal Pollution and Human Health Risk in Urban Soils of Steel Industrial City (Anshan), Liaoning, Northeast China. *Ecotoxicol. Environ. Saf.* **2015**, *120*, 377−385.

(2) Singh, B. R.; Steinnes, E. Soil and Water Contamination by Heavy Metals. In *Soil Processes Water Qual.* CRC Press, 2020, 233−271

(3) Wu, Q.; Leung, J. Y.; Geng, X.; Chen, S.; Huang, X.; Li, H.; Huang, Z.; Zhu, L.; Chen, J.; Lu, Y. Heavy Metal Contamination of Soil and Water in the Vicinity of an Abandoned E-Waste Recycling Site: Implications for Dissemination of Heavy Metals. *Sci. Total Environ.* **2015**, *506−507*, 217−225.

(4) Wan, Z.; Duan, L.; Hu, X.; Li, X.; Fang, L.; Guo, Q.; Sun, D. Removal of Mercury from Flue Gas Using Coal Gasification Slag. *Fuel Process. Technol.* **2022**, *231*, 107258.

(5) Mitra, S.; Chakraborty, A. J.; Tareq, A. M.; Emran, T. B.; Nainu, F.; Khusro, A.; Idris, A. M.; Khandaker, M. U.; Osman, H.; Alhumaydhi, F. A.; et al. Impact of Heavy Metals on the Environment and Human Health: Novel Therapeutic Insights to Counter the Toxicity. *J. King Saud Univ. Sci.* **2022**, *34*, 101865.

(6) da Silva, D. G.; Portugal, L. A.; Serra, A. M.; Ferreira, S. L.; Cerdà, V. Determination of Mercury in Rice by MSFIA and Cold Vapour Atomic Fluorescence Spectrometry. *Food Chem.* **2013**, *137* (1−4), 159−163.

(7) Lemos, V. A.; dos Santos, L. O. A New Method for Preconcentration and Determination of Mercury in Fish, Shellfish and Saliva by Cold Vapour Atomic Absorption Spectrometry. *Food Chem.* **2014**, *149*, 203−207.

(8) He, C.; Cheng, G.; Zheng, C.; Wu, L.; Lee, Y.-I.; Hou, X. Photochemical Vapor Generation and in Situ Preconcentration for Determination of Mercury by Graphite Furnace Atomic Absorption Spectrometry. *Anal. Methods* **2015**, *7* (7), 3015−3021.

(9) Gao, Z.; Ma, X. Speciation Analysis of Mercury in Water Samples Using Dispersive Liquid-Liquid Microextraction Combined with High-Performance Liquid Chromatography. *Anal. Chim. Acta* **2011**, *702* (1), 50−55.

(10) Tümay, S. O.; Yeşilot, S. Highly Selective "Turn-on" Fluorescence Determination of Mercury Ion in Food and Environmental Samples through Novel Anthracene and Pyrene Appended Schiff Bases. *J. Photochem. Photobiol. Chem.* **2021**, *407*, 113093.

(11) Mohandoss, S.; Khanal, H. D.; Palanisamy, S.; You, S.; Shim, J.-J.; Lee, Y. R. Multiple Heteroatom-Doped Photoluminescent Carbon Dots for Ratiometric Detection of Hg 2+ Ions in Cell Imaging and Environmental Applications. *Anal. Methods* **2022**, *14* (6), 635−642.

(12) Eksin, E.; Erdem, A.; Fafal, T.; Kıvçak, B. Eco-friendly Sensors Developed by Herbal Based Silver Nanoparticles for Electrochemical Detection of Mercury (II) Ion. *Electroanalysis* **2019**, *31* (6), 1075−1082.

(13) Hasanjani, H. R. A.; Zarei, K. An Electrochemical Sensor for Attomolar Determination of Mercury (II) Using DNA/Poly-L-Methionine-Gold Nanoparticles/Pencil Graphite Electrode. *Biosens. Bioelectron.* **2019**, *128*, 1−8.

(14) Abdel-Lateef, M. A. Utilization of the Peroxidase-like Activity of Silver Nanoparticles Nanozyme on O-Phenylenediamine/H2O2 System for Fluorescence Detection of Mercury (II) Ions. *Sci. Rep.* **2022**, *12* (1), 6953.

(15) Cao, X.; Zhu, L.; Yu, G.; Zhang, X.; Jin, H.; He, D. Visual and Colorimetric Determination of Mercury (II) Based on Lignosulfonate-Capped Silver Nanoparticles. *Green Chem. Lett. Rev.* **2023**, *16* (1), 2169590.

(16) Firdaus, M. L.; Fitriani, I.; Wyantuti, S.; Hartati, Y. W.; Khaydarov, R.; Mcalister, J. A.; Obata, H.; Gamo, T. Colorimetric Detection of Mercury (II) Ion in Aqueous Solution Using Silver Nanoparticles. *Anal. Sci.* **2017**, *33* (7), 831−837.

(17) Chansuvarn, W.; Tuntulani, T.; Imyim, A. Colorimetric Detection of Mercury (II) Based on Gold Nanoparticles, Fluorescent Gold Nanoclusters and Other Gold-Based Nanomaterials. *TrAC, Trends Anal. Chem.* **2015**, *65*, 83−96.

(18) Balasurya, S.; Syed, A.; Thomas, A. M.; Marraiki, N.; Elgorban, A. M.; Raju, L. L.; Das, A.; Khan, S. S. Rapid Colorimetric Detection of Mercury Using Silver Nanoparticles in the Presence of Methionine. *Spectrochim. Acta Mol. Biomol. Spectrosc.* **2020**, *228*, 117712.

(19) Chakrapani, V.; Ahmed, K. B. A.; Kumar, V. V.; Ganapathy, V.; Anthony, S. P.; Anbazhagan, V. A Facile Route to Synthesize Casein Capped Copper Nanoparticles: An Effective Antibacterial Agent and Selective Colorimetric Sensor for Mercury and Tryptophan. *RSC Adv.* **2014**, *4* (63), 33215−33221.

(20) Wang, G.-L.; Jin, L.-Y.; Wu, X.-M.; Dong, Y.-M.; Li, Z.-J. Label-Free Colorimetric Sensor for Mercury(II) and DNA on the Basis of Mercury(II) Switched-on the Oxidase-Mimicking Activity of Silver Nanoclusters. *Anal. Chim. Acta* **2015**, *871*, 1−8.

(21) Gopinath, V.; Priyadarshini, S.; Loke, M. F.; Arunkumar, J.; Marsili, E.; MubarakAli, D.; Velusamy, P.; Vadivelu, J. Biogenic Synthesis, Characterization of Antibacterial Silver Nanoparticles and Its Cell Cytotoxicity. *Arab. J. Chem.* **2017**, *10* (8), 1107−1117.

(22) Backx, B. P.; Dos Santos, M. S.; Dos Santos, O. A.; Filho, S. A. The Role of Biosynthesized Silver Nanoparticles in Antimicrobial Mechanisms. *Curr. Pharm. Biotechnol.* **2021**, *22* (6), 762−772.

(23) Ueno, K.; Sun, Q.; Misawa, H. Near-Field Spectral Properties of Nano-Engineered Metallic Nanoparticles. *Advanced Photonics 2018 (BGPP; IPR, NP, NOMA, Sensors, Networks, SPPCom, SOF)*. OSA Technical Digest (online); Optica Publishing Group: Zurich, 2018, p NoW1J.6.

(24) Pumera, M. Graphene-Based Nanomaterials for Energy Storage. *Energy Environ. Sci.* **2011**, *4* (3), 668−674.

(25) Gogotsi, Y.; Penner, R. M. Energy Storage in Nanomaterials - Capacitive, Pseudocapacitive, or Battery-Like? *ACS Nano* **2018**, *12* (3), 2081−2083.

(26) Sharma, N.; Ojha, H.; Bharadwaj, A.; Pathak, D. P.; Sharma, R. K. Preparation and Catalytic Applications of Nanomaterials: A Review. *RSC Adv.* **2015**, *5* (66), 53381−53403.

(27) Bruna, T.; Maldonado-Bravo, F.; Jara, P.; Caro, N. Silver Nanoparticles and Their Antibacterial Applications. *Int. J. Mol. Sci.* **2021**, *22* (13), 7202.

(28) Yílmaz, D. D.; Demirezen, D. A.; Mıhçıokur, H. Colorimetric Detection of Mercury Ion Using Chlorophyll Functionalized Green Silver Nanoparticles in Aqueous Medium. *Surf. Interfaces* **2021**, *22*, 100840.

(29) Huang, J.; Mo, X.; Fu, H.; Sun, Y.; Gao, Q.; Chen, X.; Zou, J.; Yuan, Y.; Nie, J.; Zhang, Y. Tyndall-Effect-Enhanced Supersensitive Naked-Eye Determination of Mercury (II) Ions with Silver Nanoparticles. *Sens. Actuators, B* **2021**, *344*, 130218.

(30) Tun, W. S. T.; Talodthaisong, C.; Daduang, S.; Daduang, J.; Rongchai, K.; Patramanon, R.; Kulchat, S. A Machine Learning Colorimetric Biosensor Based on Acetylcholinesterase and Silver Nanoparticles for the Detection of Dichlorvos Pesticides. *Mater. Chem. Front.* **2022**, *6* (11), 1487−1498.

(31) Zhao, G.; Stevens, S. E. Multiple Parameters for the Comprehensive Evaluation of the Susceptibility of Escherichia Coli to the Silver Ion. *BioMetals* **1998**, *11*, 27−32.

(32) Dawadi, S.; Katuwal, S.; Gupta, A.; Lamichhane, U.; Thapa, R.; Jaisi, S.; Lamichhane, G.; Bhattarai, D. P.; Parajuli, N. Current Research on Silver Nanoparticles: Synthesis, Characterization, and Applications. *J. Nanomater.* **2021**, *2021*, 1−23.

(33) Huang, H.; Yang, Y. Preparation of Silver Nanoparticles in Inorganic Clay Suspensions. *Compos. Sci. Technol.* **2008**, *68* (14), 2948−2953.

(34) Irshad, A.; Sarwar, N.; Sadia, H.; Riaz, M.; Sharif, S.; Shahid, M.; Khan, J. A. Silver Nano-Particles: Synthesis and Characterization by Using Glucans Extracted from Pleurotus Ostreatus. *Appl. Nanosci.* **2020**, *10*, 3205−3214.

(35) Sylvestre, J.-P.; Kabashin, A. V.; Sacher, E.; Meunier, M.; Luong, J. H. Stabilization and Size Control of Gold Nanoparticles during Laser Ablation in Aqueous Cyclodextrins. *J. Am. Chem. Soc.* **2004**, *126* (23), 7176−7177.

(36) Dang, T. M. D.; Le, T. T. T.; Fribourg-Blanc, E.; Dang, M. C. Influence of Surfactant on the Preparation of Silver Nanoparticles by Polyol Method. *Adv. Nat. Sci. Nanosci. Nanotechnol.* **2012**, *3* (3), 035004.

(37) Zeebaree, S. Y. S.; Haji, O. I.; Zeebaree, A. Y. S.; Hussein, D. A.; Hanna, E. H. Rapid Detection of Mercury Ions Using Sustainable Natural Gum-Based Silver Nanoparticles. *Catalysts* **2022**, *12* (11), 1464.

(38) Pomal, N. C.; Bhatt, K. D.; Modi, K. M.; Desai, A. L.; Patel, N. P.; Kongor, A.; Kolivoška, V. Functionalized Silver Nanoparticles as Colorimetric and Fluorimetric Sensor for Environmentally Toxic Mercury Ions: An Overview. *J. Fluoresc.* **2021**, *31*, 635−649.

(39) Jeevika, A.; Shankaran, D. R. Functionalized Silver Nanoparticles Probe for Visual Colorimetric Sensing of Mercury. *Mater. Res. Bull.* **2016**, *83*, 48−55.

(40) Bellingeri, A.; Scattoni, M.; Venditti, I.; Battocchio, C.; Protano, G.; Corsi, I. Ecologically Based Methods for Promoting Safer Nanosilver for Environmental Applications. *J. Hazard. Mater.* **2022**, *438*, 129523.

(41) Ilaria, C.; Iole, V.; Francesco, T.; Carlo, P. Environmental Safety of Nanotechnologies: The Eco-Design of Manufactured Nanomaterials for Environmental Remediation. *Sci. Total Environ.* **2022**, *864*, 161181.

(42) Thammawithan, S.; Talodthaisong, C.; Srichaiyapol, O.; Patramanon, R.; Hutchison, J. A.; Kulchat, S. Andrographolide Stabilized-Silver Nanoparticles Overcome Ceftazidime-Resistant Burkholderia Pseudomallei: Study of Antimicrobial Activity and Mode of Action. *Sci. Rep.* **2022**, *12* (1), 10701.

(43) PubChem. National Center for Biotechnology Information. PubChem Compound Summary for CID 5318517, Andrographolide, 2020;.

(44) IR Spectrum Table. https://www.sigmaaldrich.com/TH/en/technical-documents/technical-article/analytical-chemistry/photometry-and-reflectometry/ir-spectrum-table (accessed July 17, 2023).

(45) Murugan, E.; Santhoshkumar, S.; Govindaraju, S.; Palanichamy, M. Silver Nanoparticles Decorated G-C3N4: An Efficient SERS Substrate for Monitoring Catalytic Reduction and Selective Hg2+ions Detection. *Spectrochim. Acta Mol. Biomol. Spectrosc.* **2021**, *246*, 119036.

(46) Ghosh, S.; Maji, S.; Mondal, A. Study of Selective Sensing of Hg2+ Ions by Green Synthesized Silver Nanoparticles Suppressing the Effect of Fe3+ Ions. *Colloids Surf. A Physicochem. Eng. Asp.* **2018**, *555*, 324−331.

(47) Chen, L.; Qi, N.; Wang, X.; Chen, L.; You, H.; Li, J. Ultrasensitive Surface-Enhanced Raman Scattering Nanosensor for Mercury Ion Detection Based on Functionalized Silver Nanoparticles. *RSC Adv.* **2014**, *4* (29), 15055−15060.

(48) Ren, W.; Zhu, C.; Wang, E. Enhanced Sensitivity of a Direct SERS Technique for Hg 2+ Detection Based on the Investigation of the Interaction between Silver Nanoparticles and Mercury Ions. *Nanoscale* **2012**, *4* (19), 5902−5909.

(49) Schiesaro, I.; Burratti, L.; Meneghini, C.; Fratoddi, I.; Prosposito, P.; Lim, J.; Scheu, C.; Venditti, I.; Iucci, G.; Battocchio, C. Hydrophilic Silver Nanoparticles for Hg(II) Detection in Water: Direct Evidence for Mercury-Silver Interaction. *J. Phys. Chem. C* **2020**, *124* (47), 25975−25983.

(50) Prosposito, P.; Burratti, L.; Bellingeri, A.; Protano, G.; Faleri, C.; Corsi, I.; Iucci, G.; Tortora, L.; Secchi, V.; Venditti, I.; et al. Bifunctionalized Silver Nanoparticles as Hg2+ Plasmonic Sensor in Water: Synthesis, Characterizations, and Ecosafety. *Nanomaterials* **2019**, *9*, 1353.

(51) Jemal, K.; Sandeep, B. V.; Pola, S. Synthesis, Characterization, and Evaluation of the Antibacterial Activity of Allophylus Serratus Leaf and Leaf Derived Callus Extracts Mediated Silver Nanoparticles. *J. Nanomater.* **2017**, *2017*, 1−11.

(52) Mercury-Background-Document.Pdf. https://www.who.int/docs/default-source/wash-documents/wash-chemicals/mercury-background-document.pdf?sfvrsn=9b117325_4 (accessed July 17, 2023).

(53) Saenchoopa, A.; Klangphukhiew, S.; Somsub, R.; Talodthaisong, C.; Patramanon, R.; Daduang, J.; Daduang, S.; Kulchat, S. A Disposable Electrochemical Biosensor Based on Screen-Printed Carbon Electrodes Modified with Silver Nanowires/Hpmc/Chitosan/Urease for the Detection of Mercury (II) in Water. *Biosensors* **2021**, *11* (10), 351.

(54) Somé, I. T.; Sakira, A. K.; Mertens, D.; Ronkart, S. N.; Kauffmann, J.-M. Determination of Groundwater Mercury (II) Content Using a Disposable Gold Modified Screen Printed Carbon Electrode. *Talanta* **2016**, *152*, 335−340.

(55) Adarakatti, P. S.; Foster, C. W.; Banks, C. E.; Malingappa, P. Calixarene Bulk Modified Screen-Printed Electrodes (SPCCEs) as a One-Shot Disposable Sensor for the Simultaneous Detection of Lead(II), Copper(II) and Mercury(II) Ions: Application to Environmental Samples. *Sens. Actuators, A* **2017**, *267*, 517−525.

(56) Niu, X.; Ding, Y.; Chen, C.; Zhao, H.; Lan, M. A Novel Electrochemical Biosensor for Hg2+ Determination Based on Hg2+-Induced DNA Hybridization. *Sens. Actuators, B* **2011**, *158* (1), 383−387.

(57) Roushani, M.; Kohzadi, S.; Haghjoo, S.; Azadbakht, A. Dual Detection of Malation and Hg (II) by Fluorescence Switching of Graphene Quantum Dots. *Environ. Nanotechnol. Monit. Manag.* **2018**, *10*, 308−313.

(58) Chu, H.; Yao, D.; Chen, J.; Yu, M.; Su, L. Double-Emission Ratiometric Fluorescent Sensors Composed of Rare-Earth-Doped ZnS Quantum Dots for Hg2+ Detection. *ACS Omega* **2020**, *5* (16), 9558−9565.

(59) Sarkar, A.; Chakraborty, S.; Lohar, S.; Ahmmed, E.; Saha, N. C.; Mandal, S. K.; Dhara, K.; Chattopadhyay, P. A Lysosome-Targetable Fluorescence Sensor for Ultrasensitive Detection of Hg2+ in Living Cells and Real Samples. *Chem. Res. Toxicol.* **2019**, *32* (6), 1144−1150.

(60) Anitha, R.; Rajarajeswari, G. R. Selective and Ultrasensitive Spectroscopic Detection of Mercuric Ion in Aqueous Systems Using Embonic Acid Functionalized Silver Nanoparticle. *J. Cluster Sci.* **2022**, *34*, 1999−2015.

(61) Zhu, J.; Zhao, B.; Qi, Y.; Li, J.-J.; Li, X.; Zhao, J.-W. Colorimetric Determination of Hg(II) by Combining the Etching and Aggregation Effect of Cysteine-Modified Au-Ag Core-Shell Nanorods. *Sens. Actuators, B* **2018**, *255*, 2927−2935.

(62) Lobregas, M. O. S.; Bantang, J. P. O.; Camacho, D. H. Carrageenan-Stabilized Silver Nanoparticle Gel Probe Kit for Colorimetric Sensing of Mercury (II) Using Digital Image Analysis. *Sens. Bio-Sens. Res.* **2019**, *26*, 100303.

(63) Ullah, A.; Ali, I.; Ahmed, F.; Khan, S.; Shah, M. R.; Shaheen, F. Synthesis and Characterization of Peptide-Conjugated Silver Nanoparticle for Selective Detection of Hg2+ in Human Blood Plasma and Tap Water. *J. Mol. Liq.* **2019**, *296*, 112095.

(64) Saenchoopa, A.; Boonta, W.; Talodthaisong, C.; Srichaiyapol, O.; Patramanon, R.; Kulchat, S. Colorimetric Detection of Hg (II) by γ-Aminobutyric Acid-Silver Nanoparticles in Water and the Assessment of Antibacterial Activities. *Spectrochim. Acta Mol. Biomol. Spectrosc.* **2021**, *251*, 119433.

(65) Anantharaman, S.; Rego, R.; Muthakka, M.; Anties, T.; Krishna, H. Andrographis Paniculata-Mediated Synthesis of Silver Nanoparticles: Antimicrobial Properties and Computational Studies. *SN Appl. Sci.* **2020**, *2* (9), 1618.

(66) Paramelle, D.; Sadovoy, A.; Gorelik, S.; Free, P.; Hobley, J.; Fernig, D. G. A Rapid Method to Estimate the Concentration of Citrate Capped Silver Nanoparticles from UV-Visible Light Spectra. *Analyst* **2014**, *139* (19), 4855−4861.

(67) Ullrich, S. M.; Tanton, T. W.; Abdrashitova, S. A. Mercury in the Aquatic Environment: A Review of Factors Affecting Methylation. *Crit. Rev. Environ. Sci. Technol.* **2001**, *31* (3), 241−293.